This is the academic work as graduate student. Derived from it, an article is published at 2015 Phys Med Biol 60 5455.

VNIVERSITAT DE VALÈNCIA Facultat de Física

GRADO EN FÍSICA

Trabajo de Grado

Brachytherapy heterogeneity correction algorithm

Algoritmo de corrección por heterogeneidades en braquiterapia

12 de septiembre de 2011

Alumno:
Fernando Hueso González

Tutor:
Javier Vijande Asenjo

GOBIERNO DE ESPAÑA MINISTERIO DE EDUCACIÓN

Beca de colaboración del Ministerio de Educación de España en el Departamento de Física Atómica, Molecular y Nuclear de la UVEG entre el 30-11-2010 y el 30-06-2011

Contents

Abstract

The aim of this research work[1] is to study the influence of tissue heterogeneities in the dosimetry of brachytherapy. Specifically, we have developed an algorithm that takes into account calcifications located inside the prostate and corrects the reference dose in water. This algorithm is based on an analytical model and is applicable to commercial Treatment Planing Systems (TPS).

The analytical model has a consistent theoretical background, and it is based on the values of reference (the homogeneous case) and on the definition of an effective path, which scales the distances inside the calcification into larger ones. The energy released in the heterogeneous case along a certain step is associated with the energy released in water along a longer (scaled) step.

The results given by the algorithm show a remarkable agreement with the complete Monte Carlo simulations taking into account the calcifications. Several geometries and compositions of the calcification have been checked successfully.

The algorithm is also applicable for any type of heterogeneity or shielding. The real-time calculation of the algorithm makes it feasible for use in clinical treatment planning and thus for improving its quality.

Resumen

El objetivo de este trabajo de investigación[1] es el estudio de la influencia de heterogeneidades de los tejidos en la dosimetría de braquiterapia. En concreto, hemos desarrollado un algoritmo que tiene en cuenta las calcificaciones localizadas dentro de la próstata y corrige la dosis de referencia en agua. Este algoritmo está basado en un modelo analítico y es aplicable a Sistemas de Planificación del Tratamiento (TPS) comerciales.

El modelo analítico tiene un fundamento teórico consistente, y se basa en los valores de referencia (caso homogéneo) y en la definición de una longitud efectiva, que transforma el recorrido dentro de la calcificación en distancias mayores. La energía depositada en el caso heterogéneo a lo largo de un cierto tramo está asociada con la energía depositada en agua a lo largo de un tramo mayor (escalado).

Los resultados del algoritmo muestran un acuerdo significativo con la simulación de Monte Carlo completa teniendo en cuenta las calcificaciones. Se han comprobado satisfactoriamente diferentes geometrías y composiciones de la calcificación.

El algoritmo también es aplicable a cualquier tipo de heterogeneidad o blindaje. El cálculo a tiempo real del algoritmo hace factible su utilización en la planificación clínica del tratamiento y permite por tanto su mejora.

[1] Author: Fernando Hueso González - ferhue@alumni.uv.es; Tutor: Javier Vijande Asenjo - javier.vijande@uv.es

1 Introduction

Brachytherapy (BT), from the Greek word $\beta\rho\alpha\chi\nu\zeta$=brachys meaning short-distance, is a type of radiotherapy (RT) where radioactive seeds (see fig. 1) are placed surgically in the body regions affected by a tumor. This technique, whose origins date back to 1901 [1, Baltas], is frequently used nowadays for treating prostate, cervix, skin and breast cancer.

Despite the limited knowledge about radioactivity in the first years of the 20th century (Becquerel discovered it in 1896; a year after Röntgen discovered X-rays), in 1903 the first two patients were treated in St. Petersburg for facial basal cell carcinoma placing small radiation sources of radium in the cancerous area [1]. Shortly after, this treatment was also implemented in the Curie Institute of Paris, and in St. Luke's and the Memorial Hospital in New York.

FIG. 1: Brachytherapy seeds.

The widespread implementation of this procedure was slowed down due to the medical doctors' exposure to the radiation. The reason was that seeds needed to be handled manually. Nevertheless, the technological advances in radiological protection, shielding and the creation of remote afterloading systems together with the advances in imaging acquisition and more powerful computers have transformed BT in an effective and widely used treatment for many types of cancer. This technique allows the localization of the treatment (see fig. 2a), is less invasive than surgery and has lower risk of adverse side effects than other forms of RT.

In 1995, the Task Group N^{o} 43 (TG-43) of AAPM[2] Radiation Therapy Comittee published recommendations on dosimetry parameters and formalism in order to standardize the dosimetry calculation for BT treatments (see [1]). This formalism is consistent, simple to implement and is used nowadays as reference values for the dosimetry calculations. However, the formalism assumes that the predominant compound of the treated organ is equivalent to water. This premise is correct for most body tissues, but in organs like the prostate gland or the breast, the presence of calcifications (heterogeneities) affects considerably the dosimetry. In most cases, these heterogeneities are not taken into account in the planing of the treatment.

During the last 20 years, several research groups have published different works[3] and algorithms[4] in order to account for tissue heterogeneities (mainly bone, lung and air cavities like

[2] The American Association of Physicists in Medicine.
[3] See [3, Landry], [5, Sakelliou] for recent publications about heterogeneities and prostate calcifications.
[4] Recent examples of these algorithms can be consulted e.g. in [6, Julien Smeets] and [4, Emily Poon].

windpipe and rectum) and boundaries, for shielding and for applicators wall attenuation in the dosimetry calculations of the BT treatment.

However, as far as we know, no commercial Treatment Planing System (TPS) has fully introduced these corrections. For example, TPS Plato incorporates an approximate correction of colpostat vaginal shielding and TPS Abacus gives in addition a correction of scatter default for particular shielded cylinders. But, to our knowledge, no general method applicable to most cases has been developed yet. The main reasons for this low development on BT TPS, in contrast with external RT, are both medical and technical.

On the one hand, the medical experience with respect to tumor control and tolerance of organs at risk has been acquired during many years together with a fixed calculation methodology. Any substantial change on it is difficult to be accepted by the medical community, where, logically, caution prevails. For example, many centers with TPS Plato ignore the dose reduction on bladder and rectum due to the shielding of Fletcher-Williamson colpostats because it has been done successfully without these corrections for many years.

On the other hand, the main technical reasons are that most of the available algorithms are very complex and slow[5], and require to dismiss the efficient (in terms of computing time), frequently used and tested cylindrical symmetry assumption and the Dose Rate Tables (DRT) of reference. In addition, calculations are time consuming, with functions that handle primary and scatter dose components separately. The methodology of incorporating directly MC calculation on each patient might be the solution in some decades, if the computing power continues its growth. But today, this goal is neither feasible nor efficient.

Concerning the TPS, there are already a few algorithms (see [6], [4]) accounting for heterogeneities that could indeed improve dose calculation, but the ultrasound imaging technique usually used in clinical practice is not suited to be applied. In order to apply these algorithms, one needs to know both the density and the effective Z (atomic number) of heterogeneities, parameters that are not constant for calcifications. You can not get both data with ultrasound or with a classic CT, but only with a dual energy CT (as explained by [2, Chibani]). Significant differences depending on tissue composition, even when considering an homogeneous prostate, might be observed.

As in external RT with respect to lung corrections, it is a good opportunity to deal with tissue heterogeneities, the reason being that the RT Departments are in the process of incorporating a 3D anatomy with X-Ray Computed Tomography (CT) in BT, contouring bladder, urethra, rectum, and also any tissue heterogeneity, like a calcification inside the prostate gland or the breast.

Physicians are using more often applicators without shielding compatible with CT and Magnetic resonance imaging (MRI) that facilitate the former task and additionally avoid the effects of shielding. Moreover, scientific organizations (ESTRO[6], ABS[7], etc.) work on recommendations to move from the traditional ICRU[8] points to DVH[9] quantifications, which allow an easier incorporation of the correction due to tissue heterogeneities.

[5] A workaround is to take some approximations to fasten the Monte Carlo (MC) simulation (see [2, Chibani]).

[6] European Society for Therapeutic Radiology and Oncology

[7] American Brachytherapy Society

[8] International Commission on Radiation Units & Measurements. Its principal objective is the development of internationally accepted recommendations for the safe and efficient application of ionizing radiation to medical diagnosis and therapy, and radiation protection of individuals and populations.

[9] Dose Volume Histogram (see [1]). It summarizes 3D dose distributions of an arbitrary voxeliced structure in a graphical 2D format by counting the number of voxels that receive a certain dose.

As performing a MC simulation on each patient is not feasible, it is advisable to take an intermediate step that does not solve the problem completely, but contributes to palliate it and that can be incorporated nowadays in commercial TPS. This step, which is the subject of this research work, has great potential and could play a relevant role, specially in the case of prostate calcifications (see fig. 2b).

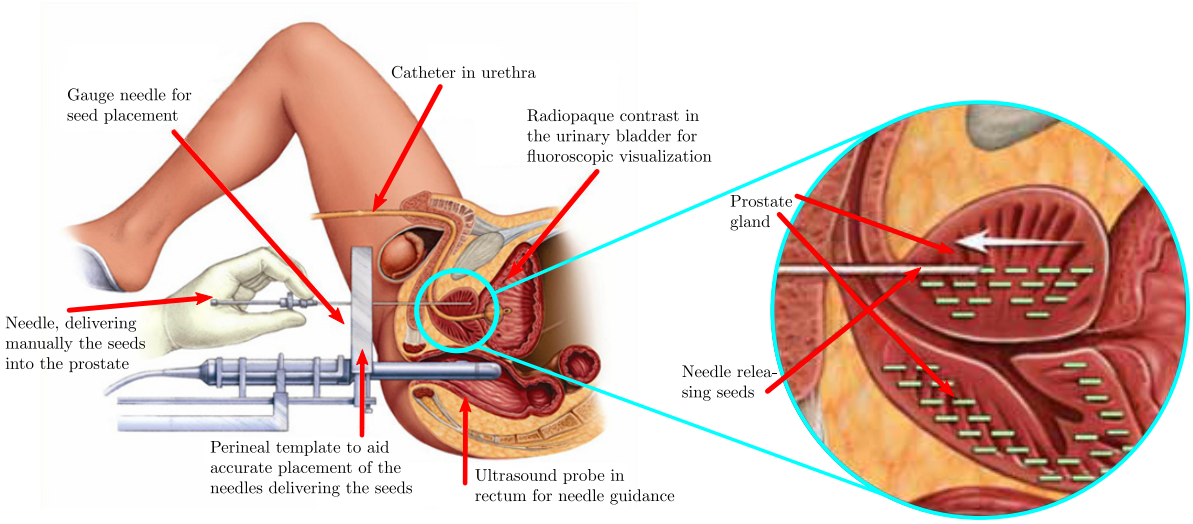

(a) Treatment with manual application of the needles.

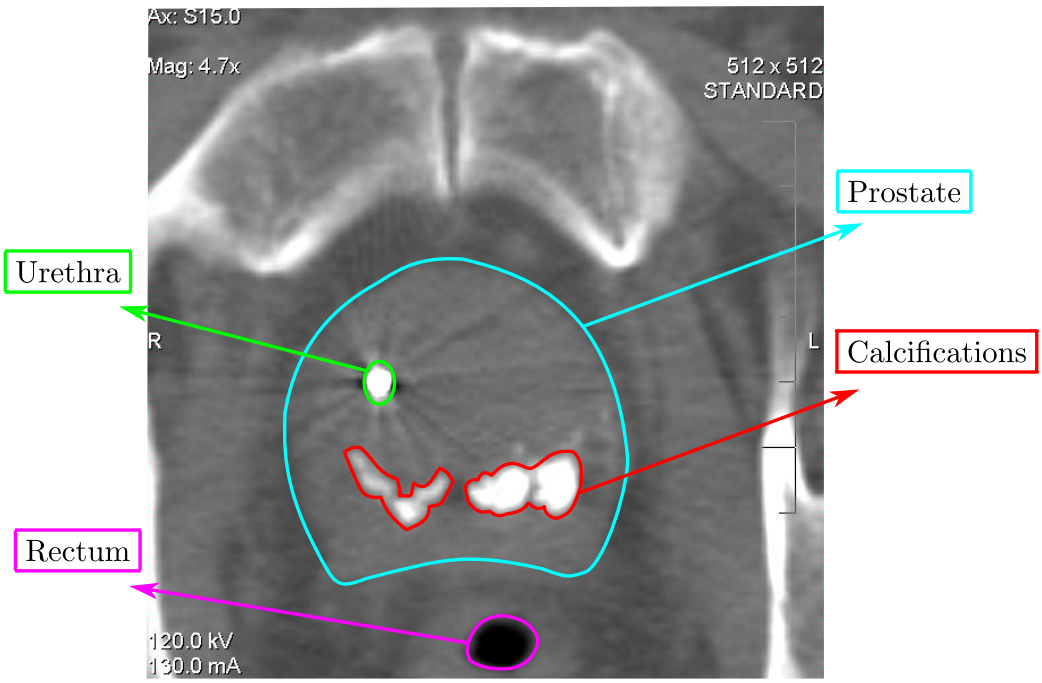

(b) Prostate calcifications of a patient. The area of the calcifications in the image is around 5 cm^2. Image of a CT, courtesy of La Fe Hospital (Valencia).

FIG. 2: Prostate brachytherapy treatment.

2 Aim and premises

The aim of this work is the correction of the dosimetry calculations in Brachytherapy (BT) due to tissue heterogeneities (particularly calcifications in the prostate) with a simple algorithm that can be easily incorporated into the Treatment Planing System (TPS) workstations of the hospitals in order to improve the quality of the BT treatment.

For achieving this goal, the algorithm has to give an estimate of the real dose received by the patient under the following conditions:

- It has to give a better estimate of the dose than the one obtained through the TG-43 formalism. The estimation does not need to be identical to the real dose, it has only to be noticeably better than the normal calculation.
- It has to be based on actual Dose Rate Tables (DRT) or TG-43 Tables published and used by all TPS to interpolate the dose once points and source have been spatially reconstructed.
- It should work over voxeliced CT slices.
- It should be applicable to general cases and geometries in any commercial TPS so that it could be incorporated in the hospitals without doing substantial changes in the TPS.
- It has to be simple and can not be time consuming.
- It should focus particularly on the prostate BT treatment for Low Dose Rate (LDR) Seeds of I-125, one of the most commonly used in the hospitals for this type of cancer.

The ultimate goal is to improve the dose calculation without relying on a slow and heavy algorithm. In other words, we can not compromise the computing time by a perfect dose estimation. It is more appropriate to develop a fast, manageable and easy to implement algorithm that gives a reasonable and proper estimate of the corrected dose, than a too precise estimate that requires large amounts of calculations (or a MC simulation) and can not be done in real-time.

The incorporation of the algorithm in patients with tissue heterogeneities would also reduce adverse side effects that might appear when the physicist corrects the distribution of the seeds inside the heterogeneity by rule of thumb.

Therefore, this is a research project focused on its application during clinical practice, which aims to improve significantly the dose calculation and thus the quality of the treatment.

3 Materials and methods

Materials The materials used for this research are personal computers, Monte Carlo Geant4 and PENELOPE codes, and associated methodology of the Medical Physics Group of the University of Valencia.

Methods The main key points and the methodology of this study are:

- To become familiar with BT treatments, the different radioactive seeds used and to study the TG-43 dosimetry formalism.
- To attend a real operation in La Fe Hospital (Valencia) for learning about the BT treatment and the TPS, as well as the image acquisition methods and delineations of organs with the computer's software.

- To develop an algorithm which corrects the dose depending on the composition of the heterogeneity.
- To draw conclusions about the robustness of the algorithm, its applicability to commercial TPS in hospitals and hypothetical generalization for other organs and treatments.

In this work, the methodology consists of the proposal of an analytical model (based on a theoretical background and the definition of effective paths) for the correction of the dose due to heterogeneities, which has to be compared with the values obtained by the MC simulation. We simulate several calcifications in a space with spherical symmetry and check which model shows a higher agreement between MC simulation and the algorithm.

Afterwards, we apply this verified algorithm to an asymmetric 3D space in order to check the validity in a more realistic case and analyze to what extent it improves the corrected dose in comparison to the dose of reference in water and the real (simulated) dose.

People involved Apart from the author of this work (Physics student), the researchers involved in this project are the group of Medical Physics of the University of Valencia - La Fe Hospital.

4 Theoretical procedure

In the first steps of the study, we analyze the dose distribution in a tissue under the following conditions and approximations:

- A single punctual radioactive seed[10], centered at the origin of a radial coordinate system ($r = 0$).
- Spherical symmetry of the surrounding tissue, whose mass density can be described with a radial function $\rho_{het}(r)$. Therefore, the whole problem is only dependent on the radial coordinate (one-dimensional problem).

The tissue is similar to an onion with three layers, as it is seen in fig. 3:

- From $r = 0$ to $r = a$, it is water.
- From $r = a$ to $r = b$, there is a calcification (relative mass density to water $\rho_m = \rho_c/\rho_w$ constant > 1). The thickness of the calcification is $t = b - a$.
- For $r > b$, it is water.

Our starting point for the algorithm are the reference values of the homogeneous case provided by a single MC simulation[11] under the conditions described in fig. 3, but with t=0 (no calcification, everything is water), that calculates the dose at a distance r from the source. These results will always be our reference values, which we use to correct the dose for different cases of a and b. An alternative would be to use the TG-43 Tables in the 1D approximation.

The purpose is to define an effective dose function that depends on the parameters of the calcification and the reference values in water, in order to avoid making a MC simulation of each kind of calcification separately and consequently saving considerable time thanks to an effective analytical algorithm.

[10] The seed is spherical and considerably small (point-like). This is a reasonable approximation, as the seeds are small in comparison with the prostate.

[11] Every MC simulation named in this document was done by the tutor of the work.

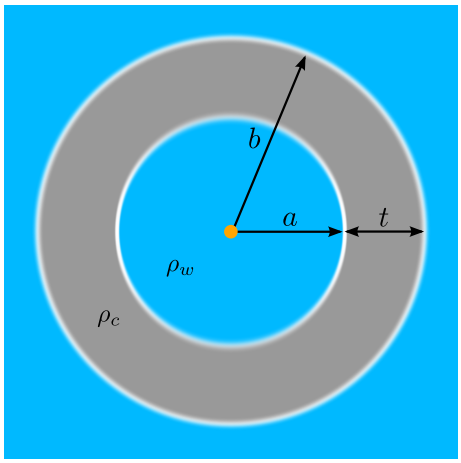

FIG. 3: Cross section of the studied tissue, with a radioactive seed in the center

We start from the conservation of energy: A seed imparts on average an energy ϵ within a volume V during its complete radioactive lifetime. If the volume is large enough ($V = \mathbb{R}^3$), there will be no energy leakage and the identity holds:

$$\epsilon_V(w) = \epsilon_V(het) \tag{1}$$

where w refers to water, that is, the homogeneous case, whereas het refers to the the heterogeneous case with a calcification. From the definition of absorbed dose D at any position $\vec{r}$ in a mass dM (volume dV) during a time interval[12]:

$$D(\vec{r}) = \frac{d\epsilon}{dM} \Longrightarrow d\epsilon = D(\vec{r})dM = D(\vec{r})\rho(\vec{r})dV \tag{2}$$

where ρ is the mass density. If energy is conserved (eq. (1)), it follows:

$$\int_V D_w(\vec{r})\rho_w(\vec{r})dV = \int_V D_{het}(\vec{r})\rho_{het}(\vec{r})dV \tag{3}$$

We integrate the angular part and since the problem has spherical symmetry (there is only dependence on the radial coordinate $r = |\vec{r}|$), then $\int dV = \int r^2 dr \int d\Omega = 4\pi \int r^2 dr$. We cancel a 4π-factor on both sides of the identity and obtain:

$$\int_0^\infty D_w(r)\rho_w(r)r^2 dr = \int_0^\infty D_{het}(r)\rho_{het}(r)r^2 dr \tag{4}$$

where the mass density $\rho_{het}(r)$ is ρ_c inside the calcification and ρ_w otherwise (see fig. 3).

The dose rate $\dot{D}_w$ (dose absorbed in unit time within a certain period of time) in the TG-43 formalism in the 1D and point-source approximation, and dismissing the anisotropy factor [1, p. 317] is defined as:

$$\dot{D}_w(r) = S_k \Lambda g_{p,w}(r)\left(\frac{r_0}{r}\right)^2 \tag{5}$$

where Λ is the dose rate constant and S_k the air kerma strength. $g_{p,w}(r)$ is the radial dose function (dimensionless) and in our case with radial symmetry is equal to $\dot{D}(r)r^2$ except for constants. We define the dose D_{het} analogously to the dose in water:

$$\dot{D}_{het}(r) = S_k \Lambda g_{p,het}(r)\left(\frac{r_0}{r}\right)^2 \tag{6}$$

[12]See Introduction to radiological physics and radiation dosimetry (p.27), Frank H. Attix.

As the dose is equal to the dose rate except for constants (assuming a time exponential decay of the source's activity), we can substitute eq. (5) and (6) in identity (4), that yields:

$$\rho_w \int_0^\infty g_{p,w}(r)dr = \int_0^\infty \rho_{het}(r) g_{p,het}(r)dr \tag{7}$$

$$\rho_w \int_0^\infty g_{p,w}(r)dr = \rho_c \int_{V_c} g_{p,het}(r)dr + \rho_w \int_{V_w} g_{p,het}(r)dr \tag{8}$$

where V_c refers to the region inside the calcification and V_w to the region filled with water. We consider a spherical shell-shaped calcification (see fig. 3) for $r \in [a, b]$. Dividing last equation by ρ_w, it follows:

$$\int_{r=0}^\infty g_{p,w}(r)dr = \int_{r=0}^a g_{p,het}(r)dr + \frac{\rho_c}{\rho_w} \int_{r=a}^b g_{p,het}(r)dr + \int_{r=b}^\infty g_{p,het}(r)dr \tag{9}$$

Until now, this derivation is purely formal and it will be the background of our algorithm, that has to estimate the real dose D_{het} in the heterogeneous case with an effective dose function[13] D_{ef} or alternatively the effective radial dose function g_{ef} given by the algorithm.

4.1 Correction algorithm

The analytical model obtained and applied in the algorithm has a consistent theoretical background and shows, as we will see in further sections, a great agreement with the values obtained with the simulation. In this section, we write the general analytical expressions obtained as a result of physical considerations.

Following the result obtained in eq. (9), we assume that the integral in the range $[0, a]$ is the same on both sides. In other words, we do not account for backscatter near the boundary (both situations are physically identical for $r < a$).

$$\int_0^a g_w(r)dr = \int_0^a g_{\text{ef}}(r)dr \Longrightarrow g_w(r) = g_{\text{ef}}(r) \quad \text{if} \quad r < a \tag{10}$$

$$\int_a^\infty g_w(r)dr = \frac{\rho_c}{\rho_w} \int_a^b g_{\text{ef}}(r)dr + \int_b^\infty g_{\text{ef}}(r)dr \tag{11}$$

Our correction algorithm is based on the definition of an effective path r_{ef}, which scales the radial distance r with a relative effective-path density ρ_r (effective parameter) of the calcification to water. This definition takes into account a greater energy deposition in tissues with higher mass density and interaction cross section than water.

Our analogy is that a higher energy deposition along a path Δr (in the calcification) is equivalent to a usual (that is, in water) energy deposition along an effective path $(\Delta r)_{\text{ef}}$ (see fig. 4). To put it another way, we transform a medium with higher density into a medium with normal density but scaled (larger) distances and associate the energy released along a path in the calcification to the energy released in a longer path in water (which is given by the reference values).

Consequently, the dose inside the calcification will rise up, and the dose after it will decrease (because of energy conservation) in comparison to the homogeneous case.

[13] From now on, we change *het* with ef (it stands for effective) when referring to the estimation given by the algorithm and with MC when referring to the MC simulation. We also simplify the notation: $g_{p,x} \equiv g_x$.

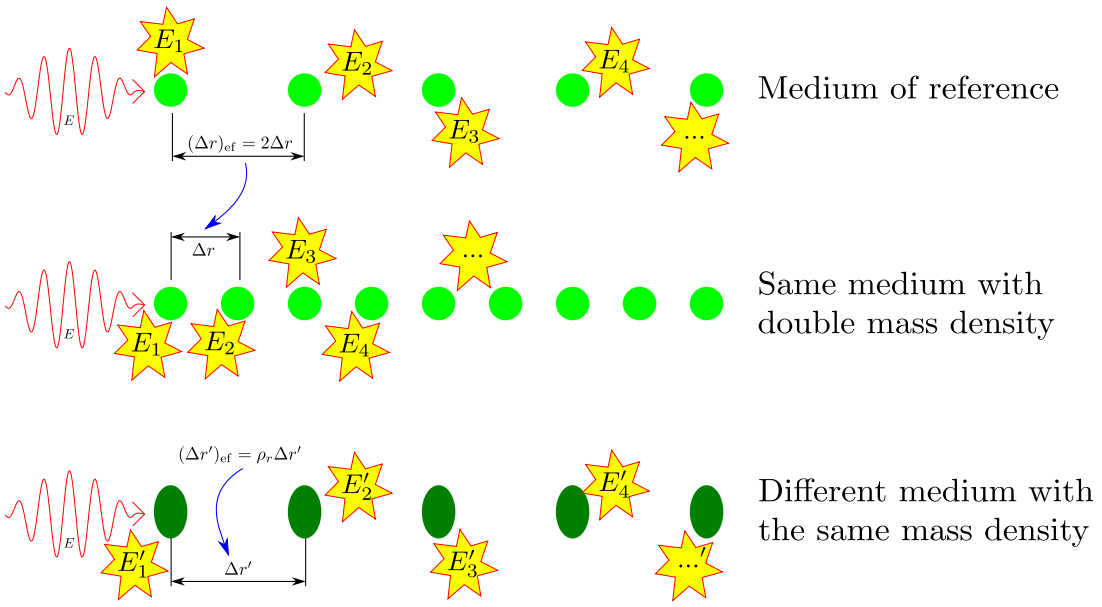

FIG. 4: Sketch of the emission energy E released by a photon in different media in a 1-D approximation. The atoms or molecules are represented as separate circles and are like obstacles for the photon, which loses energy as it collides with them. Logically, if the medium has higher density, the same number of collisions occur in a smaller range of distances. In the case of a different medium, the interaction cross section is different (atoms represented as ellipses). The extrapolation to a 3D-space with spherical symmetry is explained in footnote 16.

We define the effective radial distance as:

$$r_{\text{ef}}(r;\rho_r,a,b) = \begin{cases} r & \text{if} \quad 0 \le r \le a \\ a + \rho_r(r-a) & \text{if} \quad a < r < b \\ a + \rho_r(b-a) + (r-b) & \text{if} \quad r \ge b \end{cases} \tag{12}$$

It is a continuous function (with discontinuous derivative) that scales the distance in the calcification with the relative effective-path density ρ_r, as it can be seen in figure 5. Note that the mass density $\rho_{het}(r)$ of eq. (9) is not equal to the relative effective-path density ρ_r (the interpretation of this parameter will be discussed in subsection 4.2).

The effective dose is obtained from the dose of reference by calculating the energy released along the effective path in water and associating it to the real path in the heterogeneous case (see fig. 6).

Eq. (11) does not give us relevant information of the dependence of the curve g_{ef} with r. Therefore, it is necessary to use a differential treatment: we assume that the energy ΔE released in the heterogeneous case between r and $(r + \Delta r)$ has to be the same that the one released in water (given by the simulation of reference) between r_{ef} and $(r + \Delta r)_{\text{ef}}$.

Particularly, at the beginning of the calcification, the energy released in a range Δr between $[a, a + \Delta r]$ will be the same as the one absorbed in water between $[r_{\text{ef}}(a), r_{\text{ef}}(a + \Delta r)] = [a, a + \rho_r \Delta r]$.

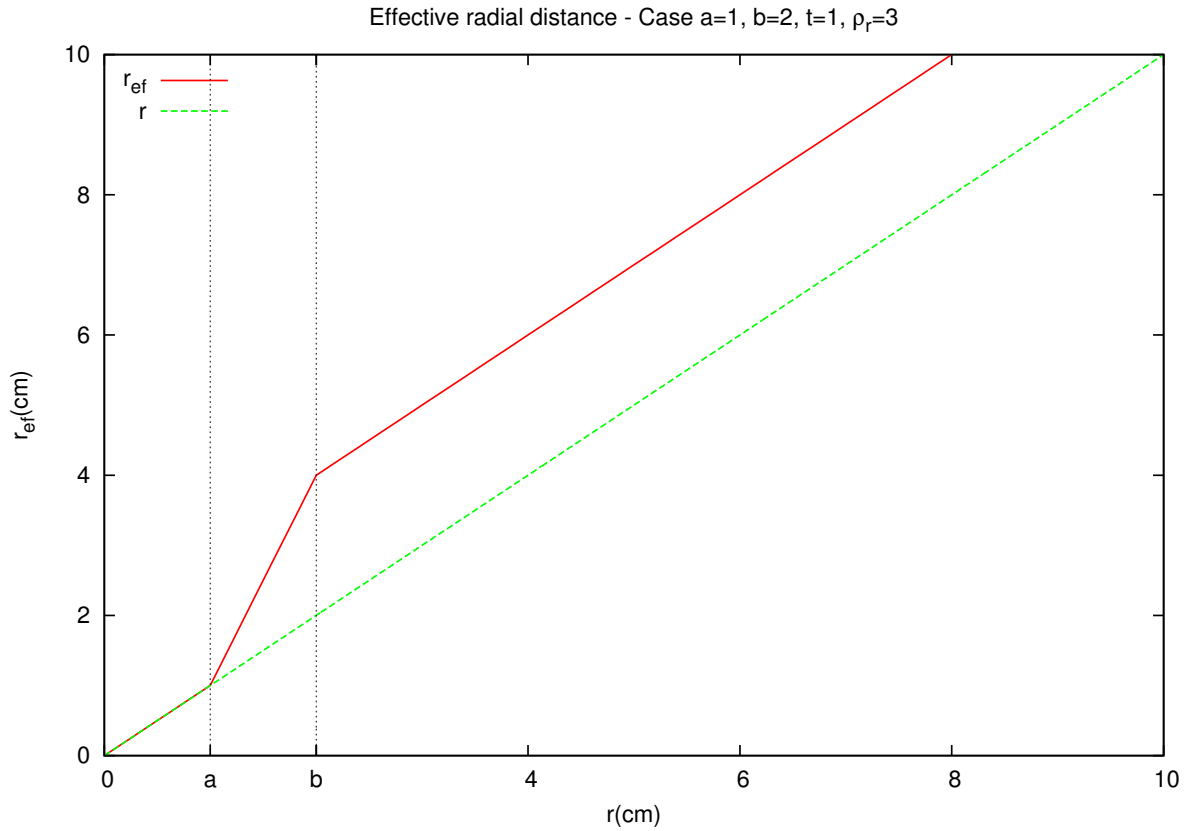

FIG. 5: Example of the calculation of the effective radial distance

In other words, part of the energy that was previously (homogeneous case) released outside the zone of the calcification remains now (heterogeneous case) inside. Mathematically, this means:

$$\frac{\rho_c}{\rho_w}\int_a^{a+\Delta r} g_{\text{ef}}(r)dr = \int_{r_{\text{ef}}(a)}^{r_{\text{ef}}(a+\Delta r)} g_w(r)dr \tag{13}$$

$$r_{\text{ef}}(a) = a \quad ; \quad r_{\text{ef}}(a+\Delta r) = a + \rho_r \Delta r \tag{14}$$

$$\frac{\rho_c}{\rho_w}\int_a^{a+\Delta r} g_{\text{ef}}(r)dr = \int_a^{a+\rho_r\Delta r} g_w(r)dr \tag{15}$$

Let us suppose Δr small, and the area under the curve rectangular (as a Riemann sum based on tagged finite partitions, with $g_{\text{ef}}(r)$ constant between r and $r+\Delta r$). Then, we can write:

$$\int_a^{a+\Delta r} g_{\text{ef}}(r)dr \simeq g_{\text{ef}}(a+\Delta r/2)\Delta r \tag{16}$$

$$g_{\text{ef}}(a+\Delta r/2) = \frac{\rho_w}{\rho_c}\frac{1}{\Delta r}\int_a^{a+\rho_r\Delta r} g_w(r)dr \tag{17}$$

Numerically, this can be generalized for the whole calcification. We obtain:

$$a + N\Delta r = b \Longrightarrow N = \frac{b-a}{\Delta r} \Longrightarrow \Delta r = \frac{b-a}{N} \quad ; \quad n \in [0, N-1] \tag{18}$$

$$g_{\text{ef}}(a+\Delta r/2+n\Delta r) = \frac{\rho_w}{\rho_c}\frac{1}{\Delta r}\int_{a+n\rho_r\Delta r}^{a+(n+1)\rho_r\Delta r} g_w(r)dr \tag{19}$$

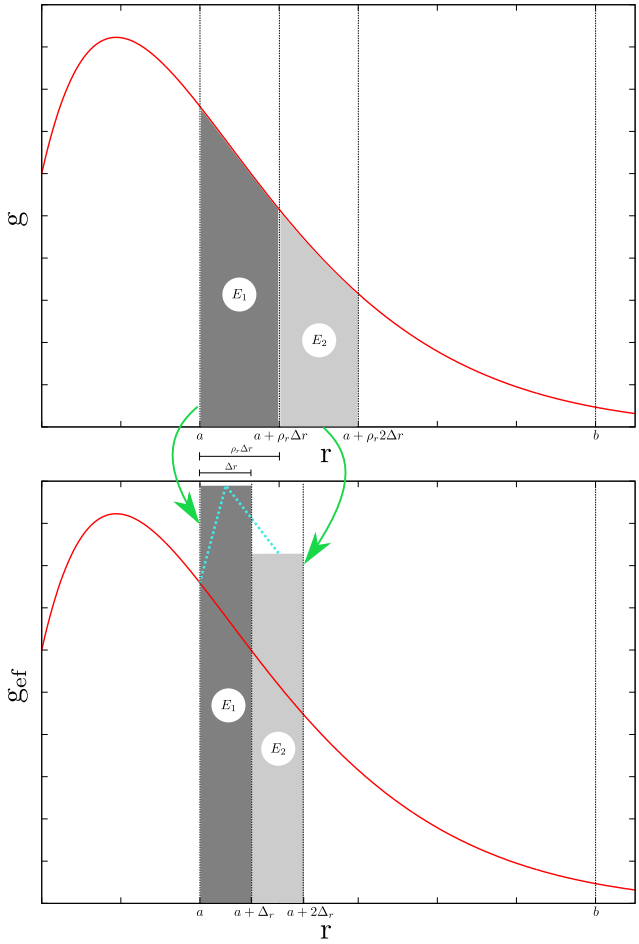

FIG. 6: Schematic illustration of the redistribution of energy inside the calcification. The blue curve represents the construction of g_{ef} with the algorithm. The areas of the transformed rectangles are not directly the energy; they are affected by a scaling factor: the relative mass density. If this factor is 1, the areas have to be similar.

In eq. (19), $\Delta r << 1$ but there is no guarantee that $\rho_r \Delta r$ is, therefore the integral has to be maintained. If we calculate the effective radial dose function at a distance r (variable change $r \to r'$, $a + \Delta r/2 + n\Delta r \to r$), we have that:

$$g_{\text{ef}}(r) = \frac{\rho_w}{\rho_c}\frac{1}{\Delta r}\int_{a+(r-\Delta r/2-a)\rho_r}^{a+(r+\Delta r/2-a)\rho_r} g_w(r')dr' \quad ; \quad a + \Delta r/2 \leq r \leq b - \Delta r/2 \tag{20}$$

Outside the calcification:

$$\int_b^{b+\Delta r} g_{\text{ef}}(r)dr = \int_{r_{\text{ef}}(b)}^{r_{\text{ef}}(b+\Delta r)} g_w(r)dr \tag{21}$$

$$r_{\text{ef}}(b) = a + \rho_r(b-a) \quad ; \quad r_{\text{ef}}(b+\Delta r) = a + \rho_r(b-a) + \Delta r \tag{22}$$

$$\int_b^{b+\Delta r} g_{\text{ef}}(r)dr = \int_{a+\rho_r(b-a)}^{a+\rho_r(b-a)+\Delta r} g_w(r)dr \tag{23}$$

Therefore, the integration interval is Δr in both cases, and as the area is considered to be rectangular, it follows that:

$$g_{\text{ef}}(b + \Delta r/2)\Delta r = g_w(a + \rho_r(b-a) + \Delta r/2)\Delta r \tag{24}$$

$$g_{\text{ef}}(b+\Delta r/2) = g_w(a+\rho_r(b-a)+\Delta r/2) \tag{25}$$

In general, we have (with $n>0$):

$$g_{\text{ef}}(b+\Delta r/2+n\Delta r) = g_w(a+\rho_r(b-a)+\Delta r/2+n\Delta r) \tag{26}$$

If we change to the continuum (variable change $b+\Delta r/2+n\Delta r \to r$):

$$g_{\text{ef}}(r) = g_w(r_{\text{ef}}(r)) = g_w(a+(b-a)\rho_r+r-b) = g_w(r+(b-a)(\rho_r-1)) \quad ; \quad r>b \tag{27}$$

Summarizing:

$$\boxed{g_{\text{ef}}(r) = \begin{cases} g_w(r) & \text{if } r<a \\ \frac{\rho_w}{\rho_c}\frac{1}{\Delta r}\int_{a+(r-\Delta r/2-a)\rho_r}^{a+(r+\Delta r/2-a)\rho_r} g_w(r')dr' & \text{if } a+\Delta r/2 \le r \le b-\Delta r/2 \\ g_w(r+(b-a)(\rho_r-1)) & \text{if } r>b \end{cases}} \tag{28}$$

Note that this function is discontinuous in order to avoid the singularities in $r=a$ and b, but its integral is well defined in the limit $\Delta r \to 0$.

For checking the validity of the result, we verify that it fulfills the identity (7), (derived directly from the conservation of energy, our starting point) making the change the other way around, that is, substituting the expressions given by eq. (28).

$$\int_0^\infty \rho_{het}(r)g_{\text{ef}}(r)dr = \rho_w\int_0^a g_w(r)dr + \rho_c\int_a^b g_{\text{ef}}(r)dr + \rho_w\int_b^\infty g_w(r_{\text{ef}})dr \tag{29}$$

where we suppose that $\Delta r << a,b,t$ so that singularities do not affect the integral. The second term is, returning to the discrete sum:

$$\begin{aligned} \rho_c\int_a^b g_{\text{ef}}(r)dr &= \rho_c\sum_{n=0}^{N-1} g_{\text{ef}}(a+(n+1/2)\Delta r)\Delta r = \rho_c\sum_{n=0}^{N-1}\Delta r\frac{\rho_w}{\rho_c}\frac{1}{\Delta r}\int_{a+n\rho_r\Delta r}^{a+(n+1)\rho_r\Delta r} g_w(r)dr \\ &= \rho_w\sum_{n=0}^{N-1}\int_{a+n\rho_r\Delta r}^{a+(n+1)\rho_r\Delta r} g_w(r)dr = \rho_w\int_a^{a+N\rho_r\Delta r} g_w(r)dr \\ &= \rho_w\int_a^{a+\rho_r(b-a)} g_w(r)dr \end{aligned} \tag{30}$$

Taking into account that $dr = dr_{\text{ef}}$ for $r>b$ (see eq. (12)), the third term is:

$$\begin{aligned} \rho_w\int_b^\infty g_w(r_{\text{ef}})dr &= \rho_w\int_{r_{\text{ef}}(b)}^\infty g_w(r_{\text{ef}})dr_{\text{ef}} = \rho_w\int_{a+\rho_r(b-a)}^\infty g_w(r_{\text{ef}})dr_{\text{ef}} \\ &= \rho_w\int_{a+\rho_r(b-a)}^\infty g_w(r)dr \end{aligned} \tag{31}$$

Then, substituting eq. (30) and (31) in (29), you proof eq. (7):

$$\begin{aligned} \int_0^\infty \rho_{het}(r)g_{\text{ef}}(r)dr &= \rho_w\int_0^a g_w(r)dr + \rho_w\int_a^{a+\rho_r(b-a)} g_w(r)dr + \rho_w\int_{a+\rho_r(b-a)}^\infty g_w(r)dr \\ &= \rho_w\int_0^\infty g_w(r)dr \end{aligned} \tag{32}$$

For different geometries (for example, many shells) in a 3D space without symmetries[14], the equations of the algorithm can be generalized into more compact expressions:

$$r_{\text{ef}}(r;\rho_r) = \int_0^r \lambda(r')dr' \tag{33}$$

[14]We trace straight rays between source and calculation point and apply the model developed for spherical symmetry. In this extrapolation, the backscatter (not included in the model) might be more important. Furthermore, the straight ray-tracing is less justified in an asymmetric situation (no compensation of the scattering on average, angular orientation is not arbitrary anymore).

which is a path integral that follows the rectilinear trajectory of a photon ray (emitted by the radioactive seed) with arbitrary orientation in a 3D space. $\lambda(r') = 1$ if $\rho_{het}(r') = \rho_w$ whereas $\lambda(r') = \rho_r$ if $\rho_{het}(r') = \rho_c$.

$$g_{\text{ef}}(r) = \begin{cases} g_w(r_{\text{ef}}) & \text{if } \rho_{het}(r) = \rho_w \\ \frac{\rho_w}{\rho_c}\frac{1}{\Delta r}\int_{(r-\Delta r/2)_{\text{ef}}}^{(r+\Delta r/2)_{\text{ef}}} g_w(r')dr' & \text{if } \rho_{het}(r) = \rho_c \end{cases} \tag{34}$$

or directly:

$$g_{\text{ef}}(r) = \frac{\rho_w}{\rho_{het}(r)}\frac{1}{\Delta r}\int_{(r-\Delta r/2)_{\text{ef}}}^{(r+\Delta r/2)_{\text{ef}}} g_w(r')dr' \tag{35}$$

It is easy to proof that this equation contains the particular case of eq. (28).

Note we assume that the mass density $\rho_{het}(r') = \rho_{het}(r)\ \forall\ r' \in [r-\Delta r/2, r+\Delta r/2]$ is either the one of water ρ_w or the one of the calcification ρ_c (a perfect piecewise constant function) along the whole step Δr. This is legitimate except in the boundaries between water and calcification, which are singular points that are not interesting for the study and that do not have any noticeable influence in the results if Δr is small in comparison to the extension of the calcification.

Eq. (35) also allows to generalize the studied system to one with smoothly changing mass densities in the space, although the correspondence of the mass density with the effective parameter ρ_r (see subsection 4.2) has to be determined precisely with a table of reference. Therefore, it could be applied for other shielding problems, boundaries, body tissues and geometries, not only for spherical calcifications in the prostate.

4.2 Physical interpretation of ρ_r

In principle, the relative effective-path density parameter ρ_r has to be adjusted manually by comparing the curve given by the algorithm with the simulation. Physically, this parameter might be closely related with the mass density and the interaction cross section.

We can interpret this parameter as a quotient between the real path and the weighted (effective) path, and thus the quotient of the mean free path of the photon of the source in water 'vs' calcification until it releases its energy E (the average emission energy) completely[15].

If we suppose (remaining in a space with spherical symmetry) an exponential attenuation [16] of the uncollided photons: $I = I_0 * e^{-\mu x}$, the mean free path is given by $1/\mu$ (where μ is the linear attenuation coefficent). Consequently, we can interpret ρ_r as:

$$\rho_r = \frac{1/\mu_{w,\bar{E}}}{1/\mu_{c,\bar{E}}} = \frac{\mu_{c,\bar{E}}}{\mu_{w,\bar{E}}} \tag{36}$$

The value of μ/ρ (X-Ray Mass Attenuation Coefficients) for elemental media can be looked up in [7, NIST Tables] at the mean energy value $\bar{E}$, where ρ is the mass density and $\rho_m = \rho_c/\rho_w$

[15] We particularize for I-125 seeds, where the predominant type of radiation is a photon with $E = 28$keV

[16] Beer-Lambert law. It refers to the intensity I transmitted through a layer of material with thickness x. Although a prerequisite of this law is that the incident rays are parallel, it can be generalized for spherical symmetry by only changing x with r. The reason is that the trajectory of the photons can be considered straight on average over the isotropic emission (we consider a space with spherical symmetry), and that the straight rays of photons suffer the same number of collisions in a sphere of radium r as in a cubic layer of thickness r. The number of particles within a sphere is proportional to r^3, whereas the number of collisions of the straight photons with these particles is directly proportional to r, because the rays are not parallel and separate from each other. Therefore, r_{ef} is proportional to r and to ρ.

the relative mass density from the calcification to water. It follows:

$$\rho_r = \frac{(\frac{\mu}{\rho})_{c,\bar{E}}}{(\frac{\mu}{\rho})_{w,\bar{E}}} \frac{\rho_c}{\rho_w} = \frac{(\frac{\mu}{\rho})_{c,\bar{E}}}{(\frac{\mu}{\rho})_{w,\bar{E}}} \rho_m \equiv (\frac{\mu}{\rho})_w^c \, \rho_m \tag{37}$$

We find reasonable that the weighted path is proportional to the relative mass density ρ_m. We can check the linearity of this equation by doing several simulations for changing values of ρ_m and obtaining manually the associated effective parameter ρ_r. Then, we can plot ρ_r as a function of ρ_m, fit it to a straight line and check if the fitted slope is similar to $\left(\frac{\mu}{\rho}\right)_w^c$ calculated with NIST Tables.

5 Results and discussion

In order to apply the algorithm developed in section 4 to a case of interest and check its validity, we will do several MC simulations and compare them with the result predicted by the algorithm.

The first example (fig. 7) shows a rather good agreement between the effective dose calculated with the algorithm and the dose given by the complete Monte Carlo simulation with a calcification.

In this simulation, we have chosen a shell-shaped calcification whose atomic composition is similar to a breast calcification detailed in [2, Chibani] with a relative mass density $\rho_c/\rho_w = 3$. For the algorithm, the effective parameter ρ_r has been adjusted checking manually which value gave a better agreement of the effective (red) with the simulated (green) curve in a larger range of distances (see fig. 7).

This proves that a simple analytical model that works in real-time (computing time about one second) gives results reasonably similar to a simulation that takes up to two days using a state-of-the-art personal computer.

Therefore, we conclude that the proposed algorithm is very appropriate and even exceeds the expectations we had when the project was started, specially considering the approximate description of the problem through effective distances and other simplifications in order to obtain a rough but reasonable estimate of the dose.

In order to make a further validation of the analytical model, we check the identity given by eq. (9) with a numerical integral of the obtained curves. In the case of fig. 7, the result is:

Curve	In	Relative deviation
g_w	5.150	Reference
g_{ef}	5.070	-1.6%
g_{MC}	5.229	1.5%

TABLE 1: Numerical check of the energy conservation in fig. 7 through the integral In indicated in eq. (9).

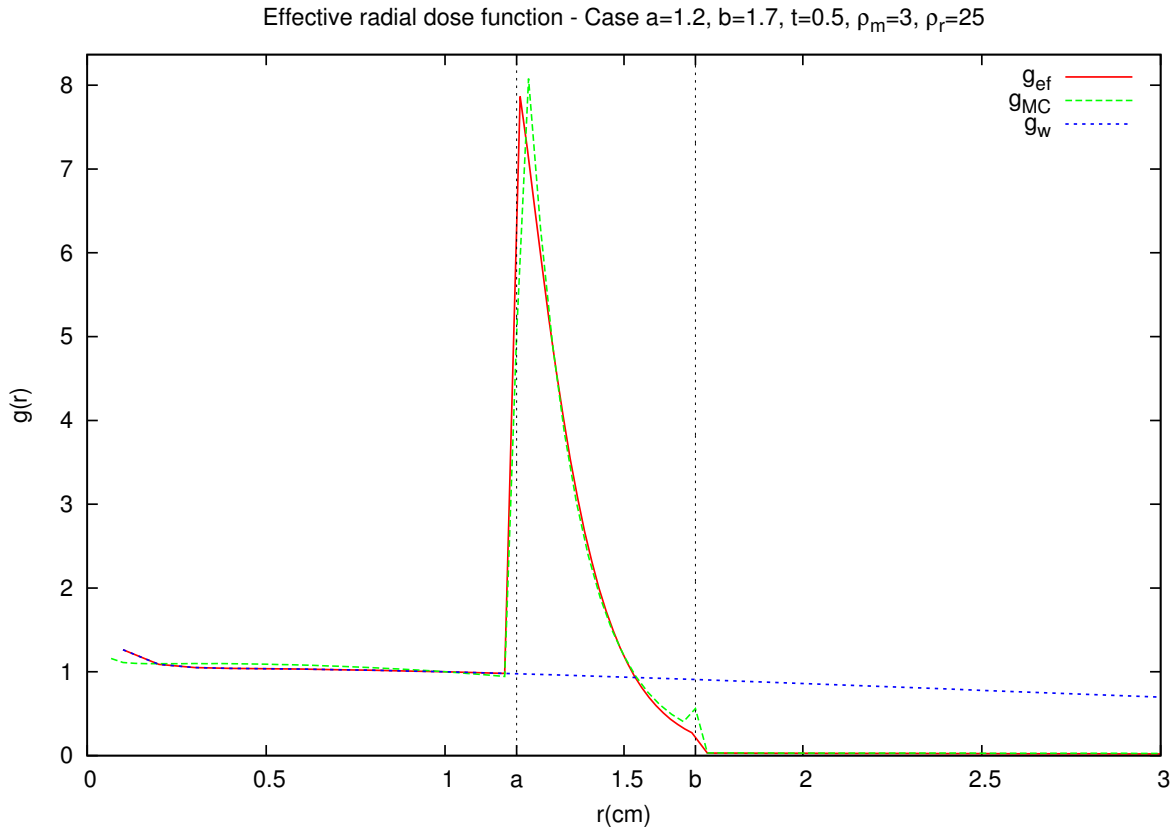

FIG. 7: Comparison of the radial dose function predicted by the correction algorithm (g_{ef}) with the Monte Carlo simulation (g_{MC}) with calcifications. Comparison with the simulation of reference in water (g_w), which is used by the algorithm. The calcification's composition is detailed in [2].

Fig. 7 shows the important role played by heterogeneities in a tissue. The absorbed dose is multiplied by 5 inside the calcification, whereas it almost sinks to zero outside it (the particular calcification chosen in this simulation acts effectively as a shielding).

When treating a tumor, this fact might be serious because the cancer cells that are outside the calcification would survive (the radiation does not reach them, they are in the "shadow") and therefore the cancer would not be completely eradicated.

While commercial TPS use the reference curve (blue) for the dosimetry and assume that the radiation goes through the calcification and releases sufficient energy after it, the real dose, given by the simulation (green), differs drastically from it by the presence of a heterogeneity with higher mass density and interaction cross section with the radiation, despite of the small thickness (5 mm) of the shell.

However, as the calculation of the dose is done real-time during the operation[17], the MC simulation is not an effective tool for dosimetry, because it takes a couple of days (for a single point-like seed and spherical symmetry geometry). In contrast, our algorithm gives real-time effective results very similar to the simulation that can be applied to more realistic cases including several seeds lasting about one second to calculate the corrected dose in any commercial

[17]The planing is done days before in the hospital, but the introduction of the seeds with needles changes the geometry of the organ and the dosimetry has to be recalculated during the operation.

computer.

Hence the importance of this algorithm in correcting the drastic effects that cause heterogeneities in tissues and the real possibility of being incorporated into commercial TPS without the drawback of excessive computing time.

We have checked the algorithm both visually and numerically (see table 1). The low relative deviation of the numerical integral is a symptom of the high degree of agreement between simulation and algorithm. Therefore, we have obtained an algorithm based on theoretical arguments whose unique free parameter is ρ_r.

For incorporating this model in commercial TPS, it would only be necessary to introduce a table of reference for different values of ρ_r according to the cases of clinical interest of the calcification's composition or relative mass density, but independently of a and b (as seen below). However, the model acquires a greater importance if we are able to physically interpret the effective parameter ρ_r and estimate its value.

5.1 Linearity of ρ_r with the mass density and estimation of $(\mu/\rho)_w^c$

In order to verify the interpretation given in subsection 4.2, we simulate a pure calcium layer for several cases of ρ_m (in fig. 7, we used a more complex composition detailed in [2]). We adjust the effective parameter manually in the algorithm and obtain several plots.

Subsequently, we represent the adjusted values of ρ_r as a function of ρ_m and check both the linearity predicted by eq. (37) and the value of $\left(\frac{\mu}{\rho}\right)_w^c$ given by the linear fit in comparison with the value given by the NIST Tables.

The agreement shown in fig. 8 is quite good. The reason of the discrepancy near the peak could be the discontinuity of the mass density in $r = a$, or the backscatter that is not taken into account in the model. However, this deviation is local and unimportant, since the agreement is very good in a large range of values of r.

Figure	Curve	In	Relative deviation
/	g_w	5.150	Reference
8a	g_{ef}	5.183	0.7%
	g_{MC}	5.316	3.2%
8b	g_{ef}	5.089	−1.2%
	g_{MC}	5.383	4.5%
8c	g_{ef}	5.011	−2.7%
	g_{MC}	5.223	1.4%
8d	g_{ef}	4.932	−4.2%
	g_{MC}	5.037	−2.2%

TABLE 2: Numerical check of the energy conservation in fig. 8 through the integral In indicated in eq. (9).

The reason of negative relative deviations (A_{ef} and $A_{MC} < A_w$) could be that the cutoff (the integral is theoretically until $r = \infty$) of the integral of the simulation and algorithm is lower than the one of the simulation of reference.

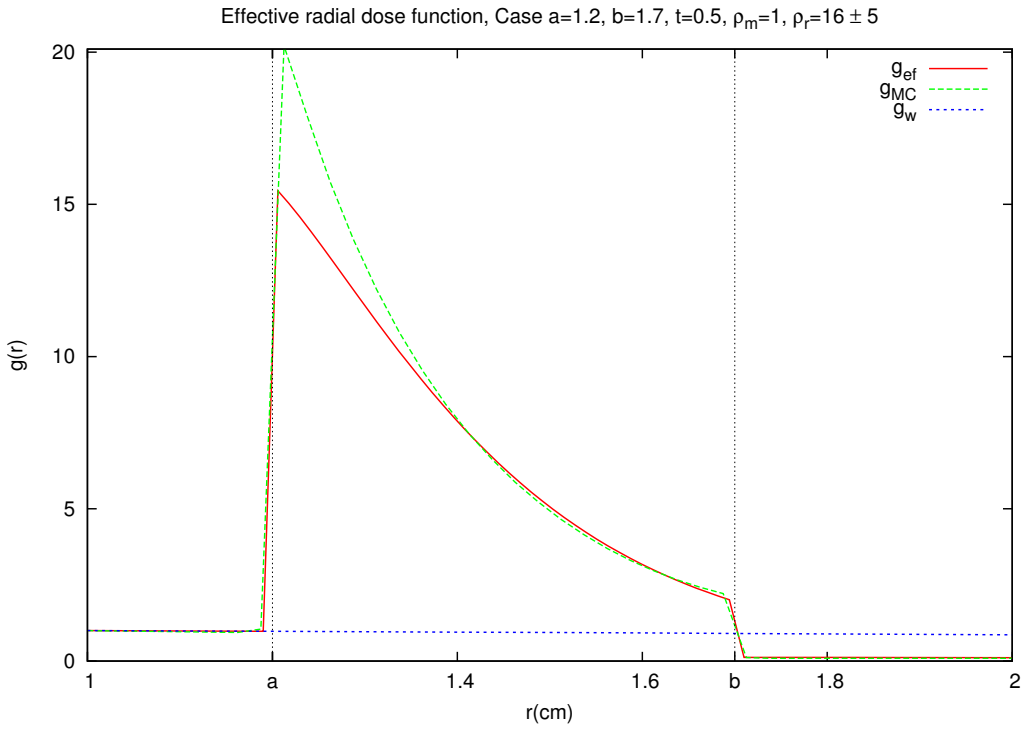

(a) Relative mass density $\rho_m = 1$

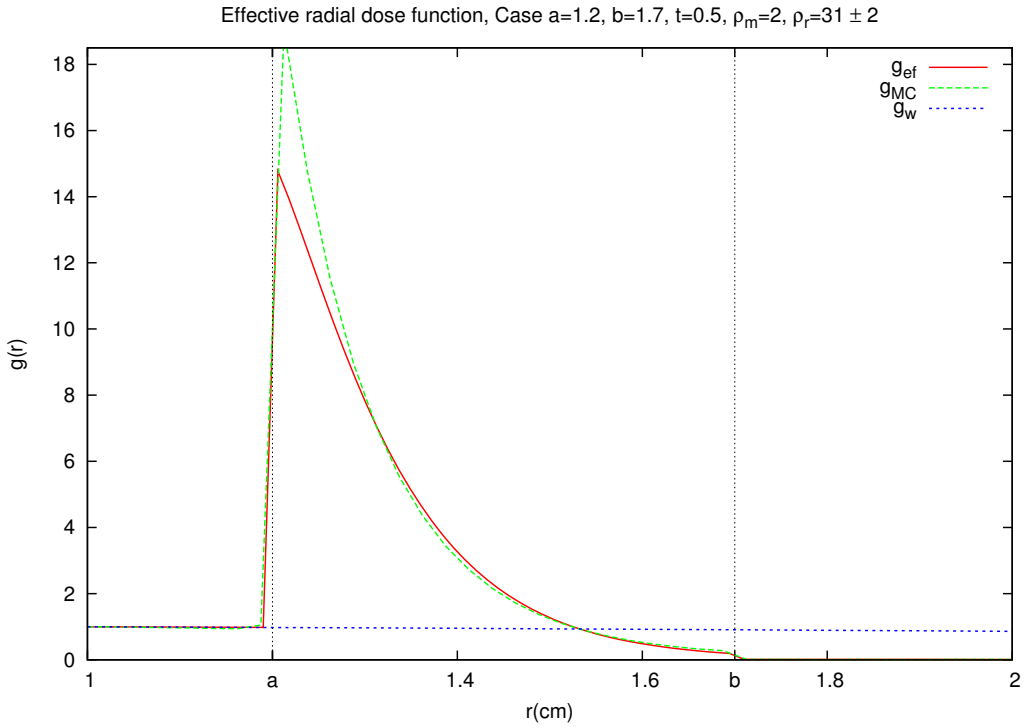

(b) Relative mass density $\rho_m = 2$

FIG. 8: Comparison of the correction algorithm (g_{ef}) (with a value of ρ_r adjusted manually) with the Monte Carlo simulation (g_{MC}) with calcifications. Comparison with the simulation in water (g_w). The effective parameter ρ_r has been adjusted manually. The calcification's composition is pure calcium.

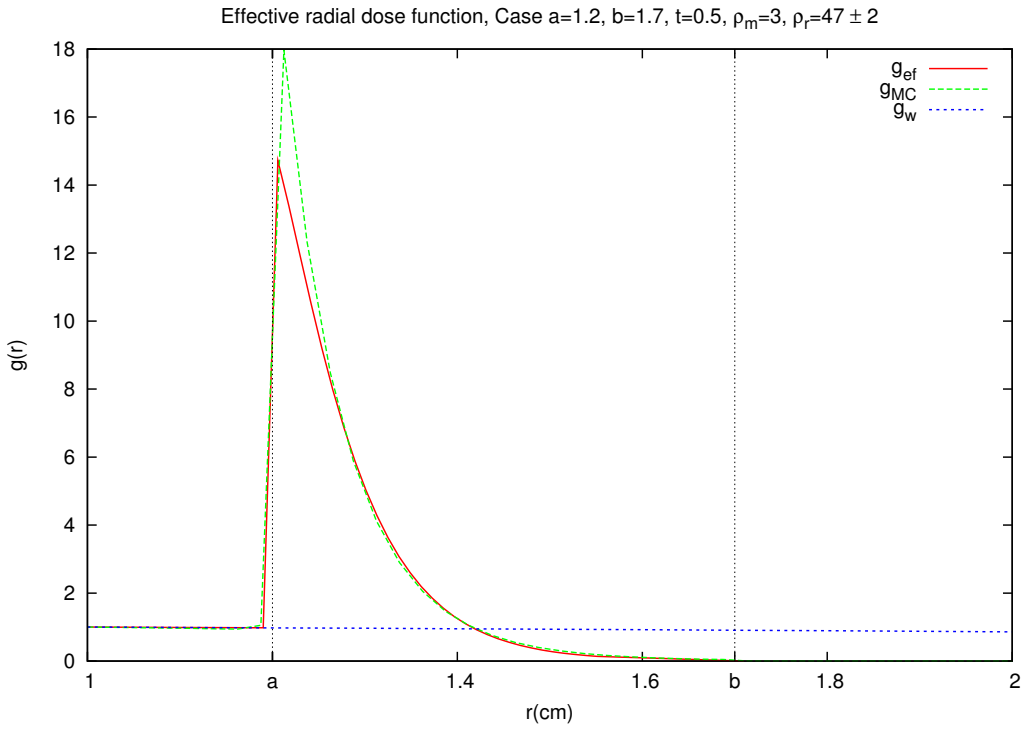

(c) Relative mass density $\rho_m = 3$

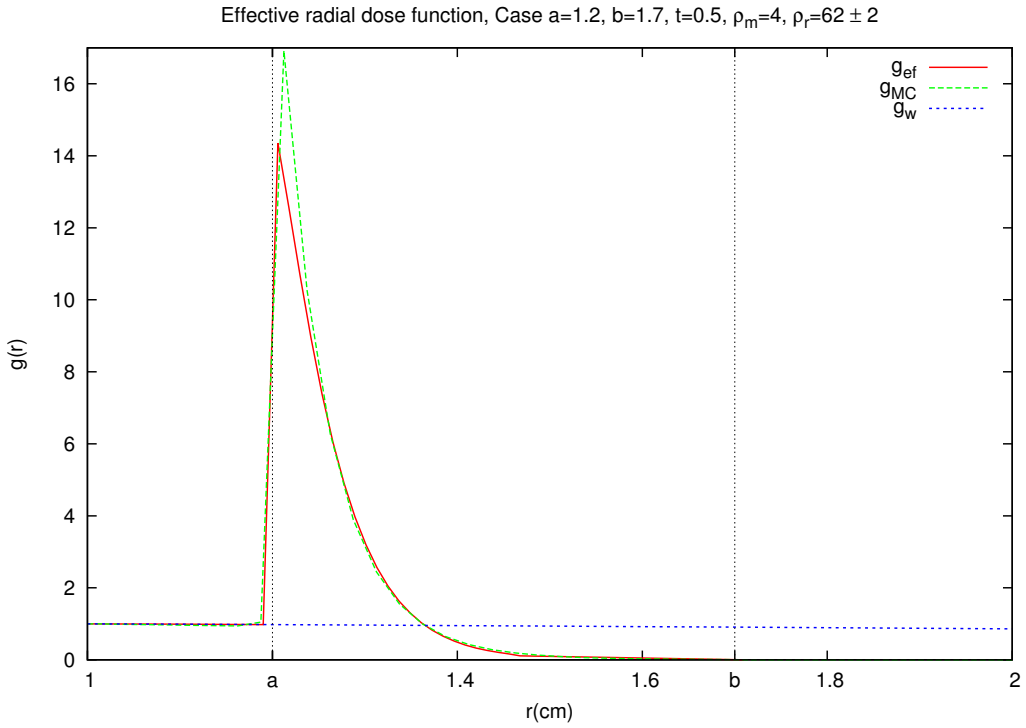

(d) Relative mass density $\rho_m = 4$

FIG. 8: Comparison of the correction algorithm (g_{ef}) (with a value of ρ_r adjusted manually) with the Monte Carlo simulation (g_{MC}) with calcifications. Comparison with the simulation in water (g_w). The effective parameter ρ_r has been adjusted manually. The calcification's composition is pure calcium.

We check the linearity predicted by eq. (37) with a linear fit for the values of ρ_r adjusted manually as a function of ρ_m, which is a fixed value chosen in each simulation.

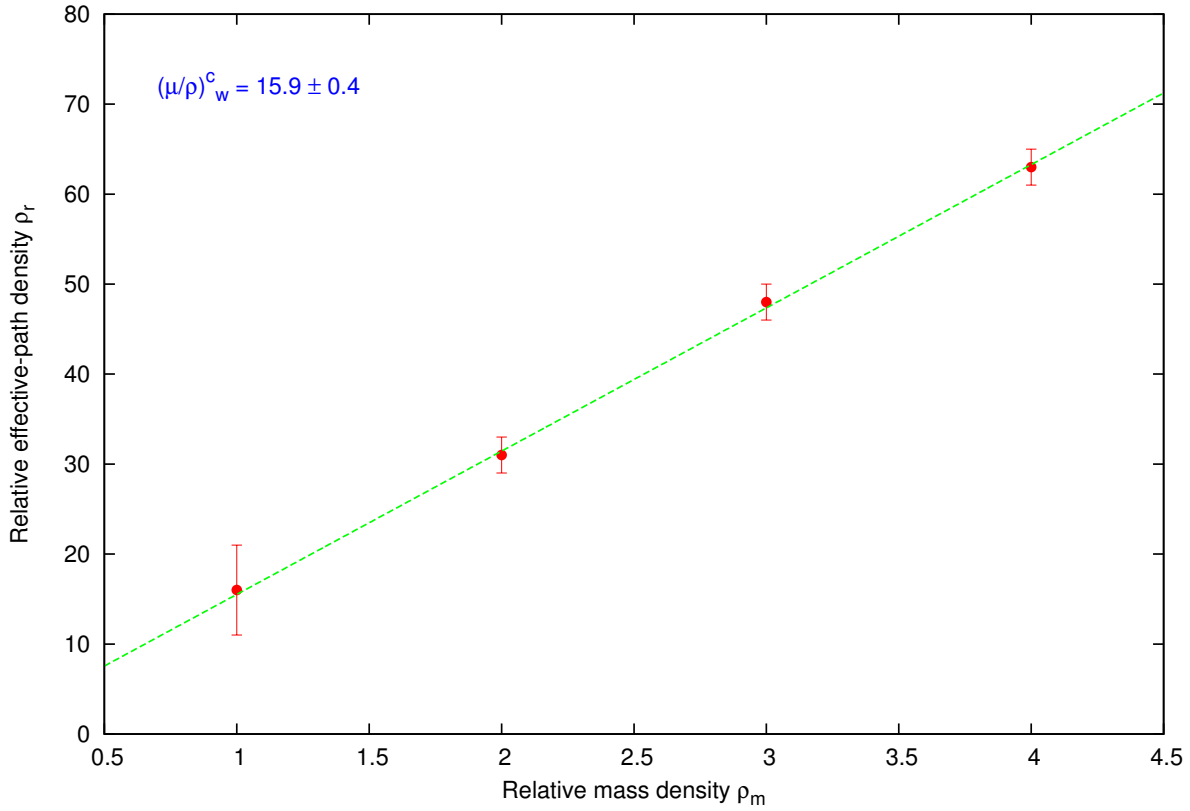

FIG. 9: Linearity of the effective parameter ρ_r with the relative mass density ρ_m. The calcification's composition is pure calcium.

The linearity becomes evident in fig. 9. Furthermore, the value of $(\mu/\rho)^c_w = 15.9 \pm 0.4$ result of the linear fit is consistent with the value given in [7] for the mean energy value of the photons of the I-125 seed: $(\mu/\rho)^c_w = 17.7 \pm 0.2$.

The reason of the slight disagreement could be either the approximation of taking constant μ/ρ at the mean energy value (although the radiation could lose only part of its energy in successive collisions and scattering), or the neglecting of the contribution of the electrons to the radiation.

In conclusion, the value given by eq. (37) is a good estimate, it gives the correct order of magnitude, but the most acute fit has to be found manually by comparing it with the Monte Carlo simulation or by adding more considerations to the theoretical model underlying the algorithm.

In our opinion, the most functional procedure for incorporating this algorithm in the TPS of hospitals is to adjust this effective parameter (manually, comparing with a MC simulation with spherical symmetry) for various compositions of clinical interest and to build a table of reference for the algorithm, values that could be compared with those obtained by NIST Tables.

5.2 Independence of ρ_r on the geometry of the calcification

Until now, we have checked the algorithm only for a single geometry of the calcification (a and b are always the same) and changing compositions and mass densities. In order to rule out that the agreement is accidental with the particular geometry and to verify the robustness of the algorithm, we have to make further simulations changing the size but not the composition of the calcification.

We expect that the algorithm is also applicable in these cases with the previously adjusted values of ρ_r. In order to verify this independence of ρ_r on a and b, we repeat the cases 8c and 8d changing those two parameters.

As it can be seen in fig. 10, the new manually adjusted ρ_r values are the same as the previous ones. Therefore, we can say that the algorithm is robust and can be applied for many cases, and not only for a calcification but for other type of tissue heterogeneities or boundaries.

Of course, the number of cases studied is low and limited by the time spent in this research, because every MC simulation (essential in each case for comparing it with the analytical model) lasts about two days. This algorithm has to be checked with more geometries and compositions, but the first results obtained are hopeful and invite to be optimistic.

Figure	Curve	In	Relative deviation
/	g_w	5.150	Reference
10a	g_{ef}	4.990	-3.1%
	g_{MC}	5.038	-2.2%
10b	g_{ef}	4.911	-4.6%
	g_{MC}	4.919	-4.5%

TABLE 3: Numerical check of the energy conservation in fig. 10 through the integral In indicated in eq. (9).

5.3 3D case without symmetries

In this section, we apply the algorithm to a case more similar to real prostate calcifications, as it can be seen in fig. 2b. We have placed two calcifications and one radioactive seed in a 3D space of a size similar to a prostate gland. Both calcifications have the same composition but different size. The composition chosen this time is neither the one from [2, Chibani] nor pure calcium, but a specific composition for prostate calcifications detailed in [6, Smeets]. The relative mass density $\rho_m = 1.1$ is measured in La Fe Hospital from a real CT of a patient with prostate calcifications (see fig. 2b).

The option of delimiting with the computer the contour of the calcification in the medical ultrasonography analogous to the delimitation of rectum and urethra should be added to the TPS software, and also the specification of its composition and mass density. These parameters should be associated with a certain value of ρ_r in a table of reference.

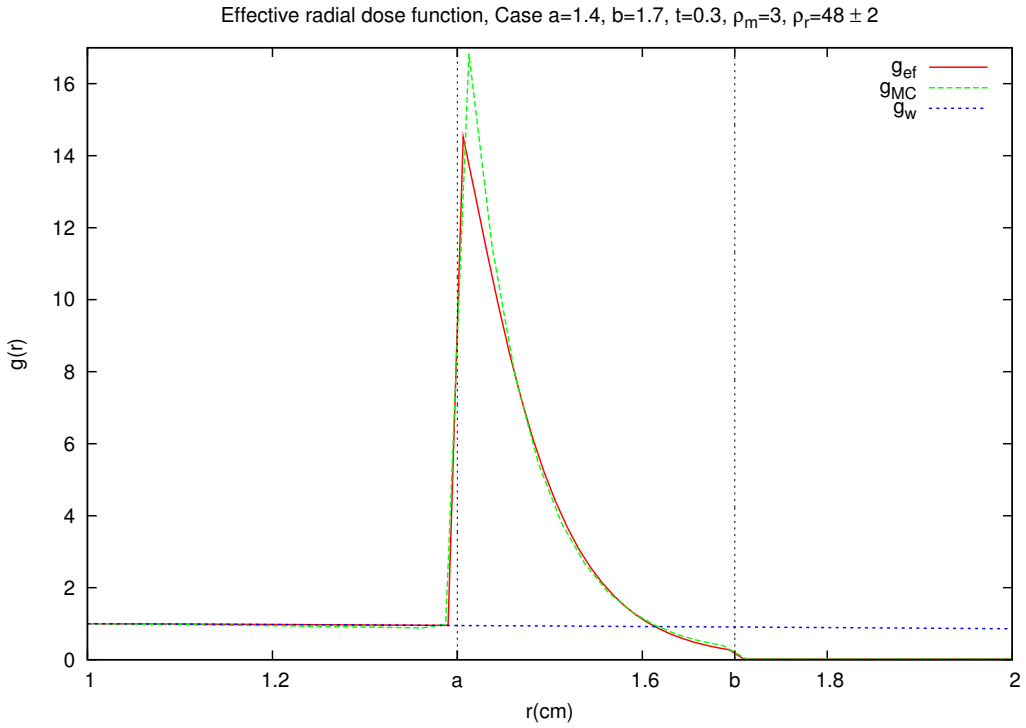

(a) Relative mass density $\rho_m = 3$

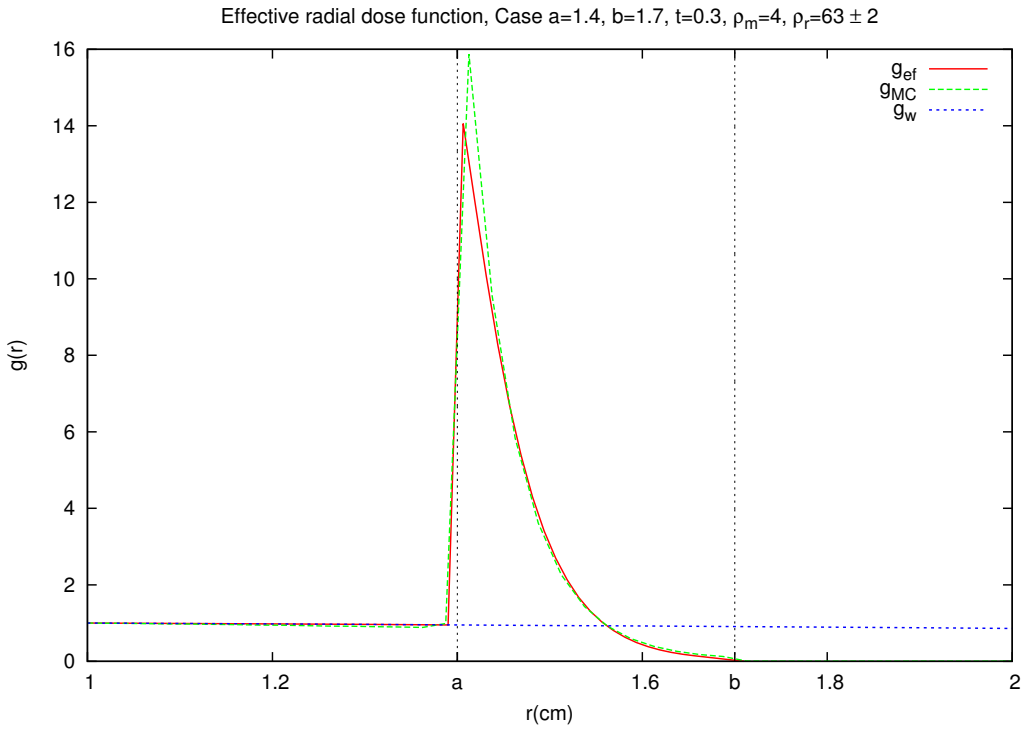

(b) Relative mass density $\rho_m = 4$

FIG. 10: Comparison of the correction algorithm between fig. 8c, 8d and 10a, 10b. The manually adjusted ρ_r parameters are the same independently from a and b in each case. The calcification's composition is pure calcium.

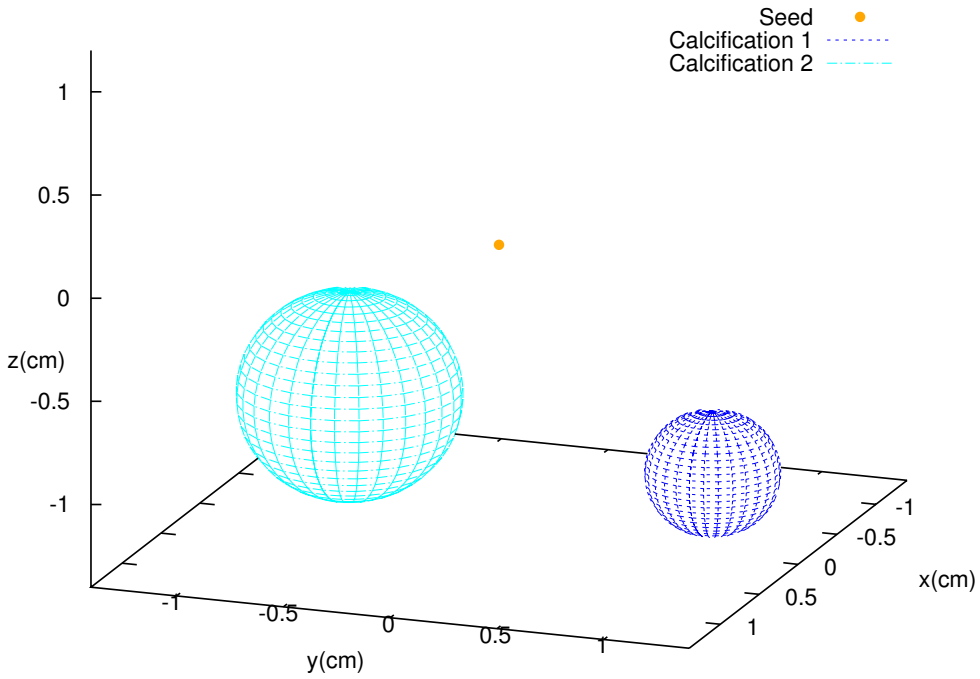

FIG. 11: Distribution of the calcifications without symmetries inside the cubic prostate and with a radioactive seed at the origin of the cartesian coordinate system. The two calcifications (1 and 2) are compact spheres of radia $R_1 = 0.3$ cm, $R_2 = 0.5$ cm and centered at $x_1 = 0$ cm, $y_1 = 1$ cm, $z_1 = -1$ cm and $x_2 = 0$ cm, $y_2 = -0.7$ cm, $z_2 = -0.8$ cm. The calcification's composition is given in [6]. We fix the parameters $\rho_m = 1.1$ and $\rho_r = 5.3$.

In order to obtain the value of ρ_r for this new composition, we repeat the usual proceeding: we make a simulation with spherical symmetry and adjust the parameter manually. The results can be seen in figure 12.

Curve	In	Relative deviation
g_w	5.150	Reference
g_{ef}	5.157	0.1%
g_{MC}	5.065	−1.6%

TABLE 4: Numerical check of the energy conservation in fig. 12 through the integral In indicated in eq. (9).

The agreement is notable and the value obtained for the effective parameter is

$$\rho_r = 5.3 \pm 0.5$$

The predicted value of ρ_r according to eq. (37) and using the attenuation coefficients calculated by Penelope in the MC simulation (NIST Tables are not useful for complex compositions), has the same order of magnitude: $\rho_r = 4.4 \pm 0.2$.

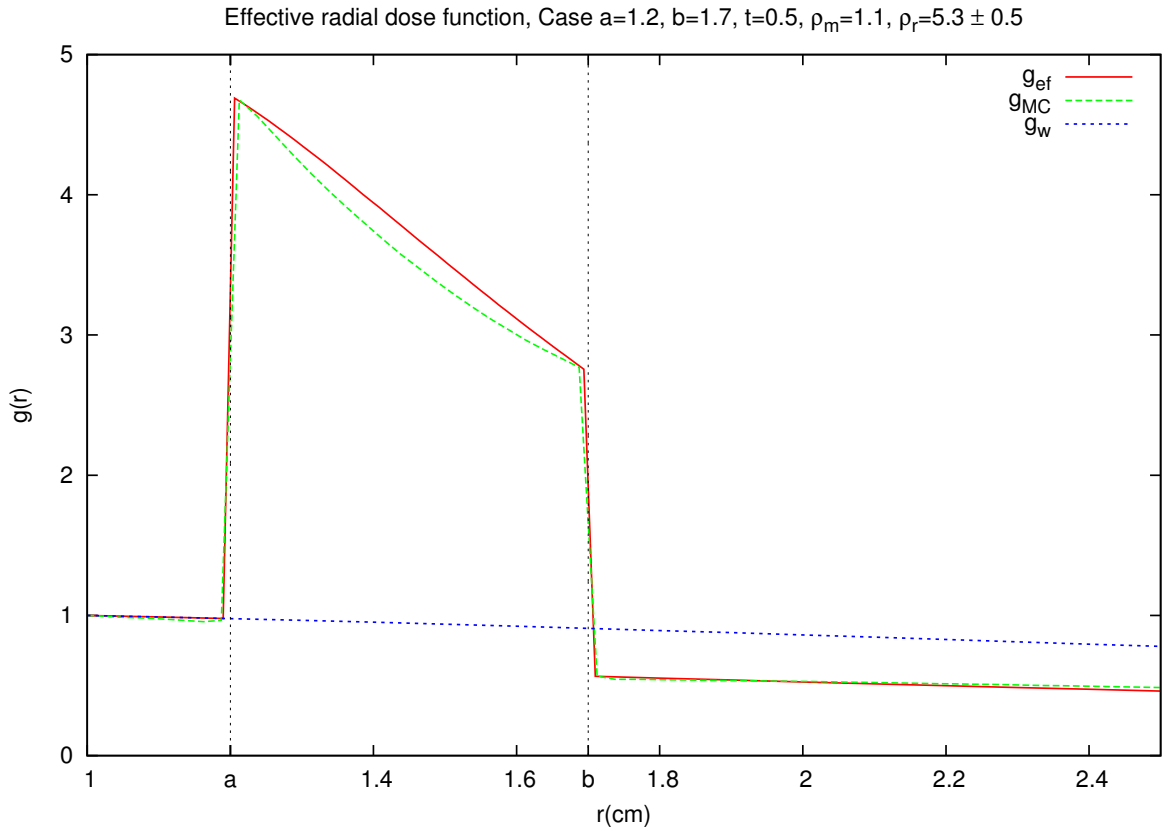

FIG. 12: Comparison of radial dose function predicted by the correction algorithm (g_{ef}) with the Monte Carlo simulation (g_{MC}) with calcifications. Comparison with the simulation of reference in water (g_w), which is used by the algorithm. The calcification's composition is detailed in [6].

In the 3D case, we expect that the calcifications shield the radiation and creat "cold spots" in the absorbed dose heat map, according to the behaviour of the curve in fig. 12 for distances greater than b.

For analyzing the effect of calcifications, we calculate the dose in eV/g per history[18] (not the radial dose function) in different cutting planes. Below we represent only the planes that are illustrative and show better the effect of heterogeneities in the dose heat map. The homogeneous case is compared with the case with calcifications.

In fig. 13b, the presence of the calcifications origins an increase in the dose inside them (hot spot) in comparison with fig. 13a, analogous to the peak between a and b of fig. 12. "Behind" the calcifications, one can see a decrease of the dose: the calcifications origins a "cold spot".

In the case of fig. 14b, we are in the "shadow" of the calcification, that origins a decrease of the dose and cold spots (blue) that are not present in fig. 14a, for example at the top and bottom of the figure. These spots are the effect of both calcifications. These results (fig. 14) are consistent with the effects observed in the spherical geometry. In the analogy of fig. 12, we are at distances greater than b, where the effective (red) curve is under the reference (blue) curve.

[18]The dose units are the one of the MC simulation (eV/g per history). The values $g(r)/r^2$ of the algorithm and reference in water are multiplicated with a conversion factor obtained by comparing with the simulation. The constants S_k and Λ are not specified.

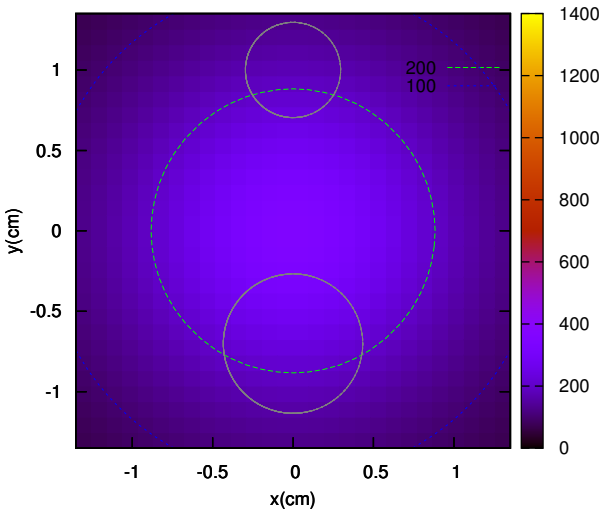

(a) Dose without taking into account the effect of calcifications

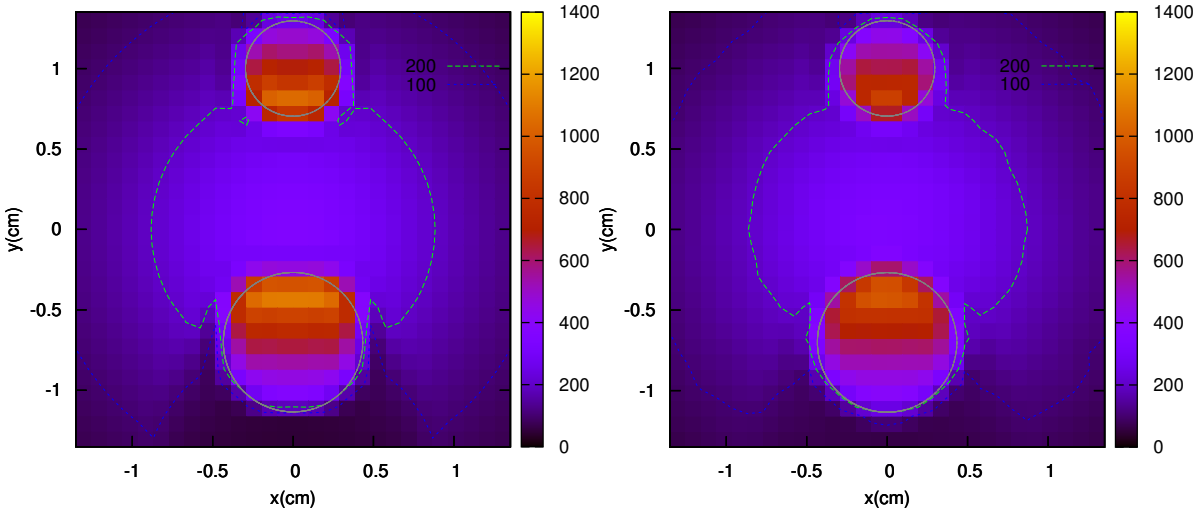

(b) Effective dose taking into account the effect of calcifications with the algorithm

(c) Dose taking into account the effect of calcifications in the MC simulation

FIG. 13: Dose heat map (eV/g per history) in cutting plane $z = -1.05$cm. The dashed lines represent isodose curves. The gray lines represent the cross section of calcifications 1 and 2 (see fig. 11). The plane $z = -1.05cm$ cuts them under their center.

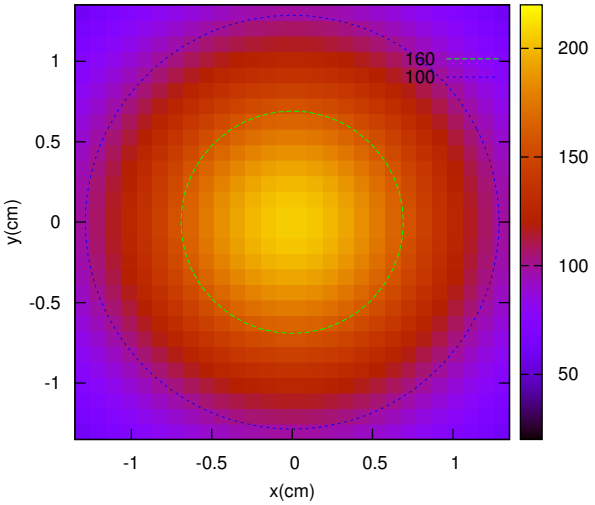

(a) Dose without taking into account the effect of calcifications

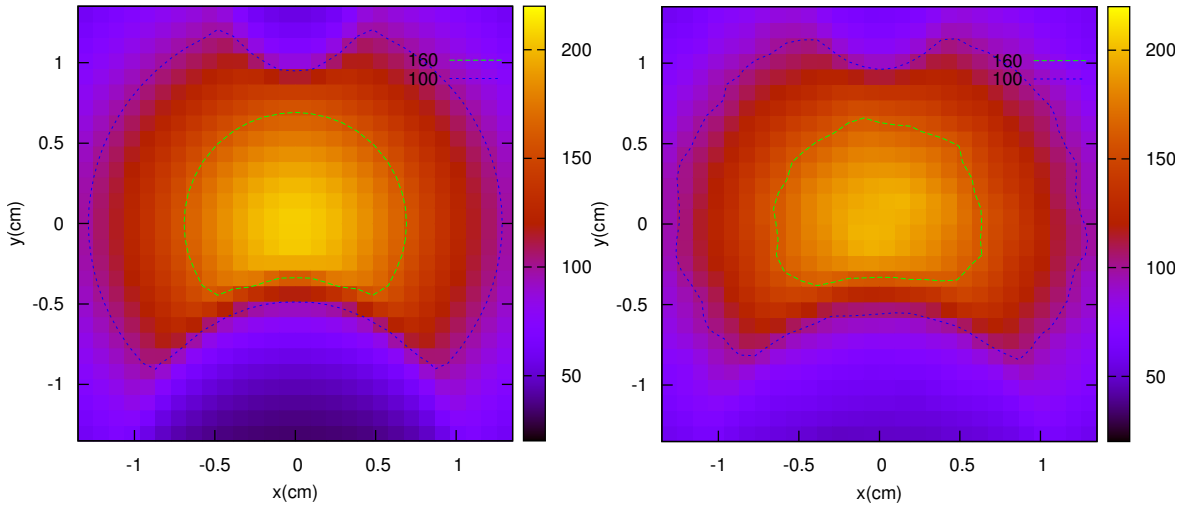

(b) Effective dose taking into account the effect of calcifications with the algorithm

(c) Dose taking into account the effect of calcifications in the MC simulation

FIG. 14: Dose heat map (eV/g per history) in cutting plane $z = -1.35$ cm. The dashed lines represent isodose curves. The plane $z = -1.35$ cm does not cut any calcification (see fig. 11).

The result of the simulation (around 3 weeks of computing time) of this case without symmetries (more time consuming) is seen in fig. 13c and 14c. We check visually (following the countour lines) that the algorithm (fig. 13b and 14b) agrees reasonably with the MC simulation. As the results show a good agreement, it is reasonable to think that it can be applied for the 40 seeds that are placed inside the prostate in each treatment (the real case).

A simulation of 40 seeds is not feasible with the computers that are available to us in the University and the result given by the algorithm (which computes without problems the case with all these seeds) can not be checked. Therefore, the verification of the model has to be done only with one seed and extrapolate the validity range for more seeds, which is reasonable if we dismiss interseed attenuation (the problem is additive).

5.4 Comments on the model underlying the algorithm

Strengths

- It conserves the energy.
- The effective parameter ρ_r is only dependent on the composition and proportional to the mass density, but is independent on the geometric parameters of the calcifications a and b.
- The agreement between model and simulation exceeds the expectations of this work.
- The model relies on a consistent physical background, where every parameter is physically interpreted.
- It provides a fast, effective and easy to implement algorithm that can be incorporated in commercial TPS.
- The algorithm is robust and has been checked for several heterogeneity geometries and compositions.

Weaknesses

- It does not take into account backscatter inside the calcification.
- The boundaries of the calcification are singular points where the dose can not be calculated.
- The algorithm assumes a point-source approximation and does not consider interseed attenuation.
- The agreement between the simulation and algorithm (green and red curves) inside the calcification is good (the step Δr has to be small), except near the dose peak in $r = a$. This deviation is not relevant for our purpose, as it is explained in section 2.
- The agreement of simulation and algorithm is strongly dependent on the effective parameter ρ_r. The model does not predict an optimum value of ρ_r, that has to be adjusted manually with the results of the simulation. An interpretation and estimate of this parameter is given in subsection 5.1.
- The theoretical background is based on arguments for a 1D space (fig. 4) and formalism, which is extrapolated directly to a 3D space with spherical symmetry (and validated with a MC simulation). The same happens with the interpretation of ρ_r in subsection 4.2 and the Beer-Lambert law.
- We extrapolate the algorithm verified for a 3D space with spherical symmetry to an asymmetric situation described in fig. 11, dismissing the effect of scattering of rays and a more important influence of backscatter.

6 Conclusions

An analytical dose calculation algorithm has been developed successfully for BT treatment in order to account for tissue heterogeneities like calcifications in the prostate. The model, which has a consistent physical background, has been verified using spherical symmetry geometries and also an asymmetric situation, and has shown a good agreement with MC simulations. Furthermore, the model is able to give a good estimate of the effective parameter ρ_r.

In other words, an analytical model that works real-time gives results reasonably similar to a MC simulation that takes up to two days. Apart from the high calculation efficiency of the algorithm, it is simple, light and might be implemented in commercial TPS (e.g Plato), in contrast to a complete MC simulation, that can not operate real-time.

This algorithm is not useful for patients that do not present tissue heterogeneities, but for those that do, it accounts for an important correction that nowadays is mostly dismissed. The effect of calcifications is not negligible but drastic, as seen in fig. 7. Therefore, we hope that (after further studies) it can be incorporated gradually in medical practice.

Although the research has focused on prostate calcifications, the theoretical model is general and can be applied for other tissue heterogeneities and shielding in RT treatments. There is no restriction of the type of heterogeneity, the only parameters that need to be determined are the relative mass density ρ_m and the effective parameter ρ_r. The first one has to be measured from imaging techniques and the second one can be obtained with the MC simulation with spherical symmetry.

The number of studied cases is yet low and limited by the time spent in this research. The algorithm has to be verified for more 3D asymmetric geometries (with a DVH) in the near future and for real seeds (not point-like).

In addition, a study in depth of the relationship between the composition of the heterogeneity and the effective parameter ρ_r should be done in order to establish a table of reference and consensus. The results of the simulation should be also checked experimentally using real phantoms and seeds.

It is also necessary to study how to obtain the typical parameters of the calcification (composition, mass density, electronic density, effective Z, etc.) from the imaging techniques usually used in clinical practice, or how to modify them for measuring these values.

In conclusion, the incorporation of this model in the dosimetry of patients with heterogeneities is feasible medium-term and it would improve significantly the dosimetry planing, reduce adverse side effects and increase the quality of the BT treatment.

Conclusiones

En este trabajo se ha desarrollado satisfactoriamente un algoritmo para el cálculo analítico de dosis en el tratamiento de braquiterapia con el fin de tener en cuenta las heterogeneidades en tejidos, como por ejemplo las calcificaciones en la próstata. El modelo, que tiene un fundamento teórico consistente, se ha verificado para un geometría con simetría esférica y también para una situación asimétrica, y ha mostrado un alto acuerdo con las simulaciones de MC. Además, el modelo es capaz de dar una buena estimación del parámetro efectivo ρ_r.

En otras palabras, un modelo analítico que opera a tiempo real da resultados razonablemente similares a una simulación de MC que dura hasta dos días. Aparte de la gran eficiencia de cálculo del algoritmo, éste es simple, ligero y podría ser introducido en TPS comerciales (por ejemplo en Plato), a diferencia de una simulación de MC completa, que no puede dar resultados a tiempo real.

Este algoritmo no es útil para pacientes que no presentan heterogeneidades en su tejido, pero para aquellos que sí, éste da cuenta de una corrección importante que generalmente se obvia. El efecto de las calcificaciones no es despreciable sino drástico, como se observa en la figura 7. Por tanto, confiamos en que (tras posteriores estudios) se pueda incorporar gradualmente a la rutina clínica.

Aunque la investigación se ha centrado en calcificaciones en la próstata, el modelo teórico es general y puede ser aplicado en otro tipo de heterogeneidades y blindajes en tratamientos de RT. No existe restricción sobre el tipo de heterogeneidad, los únicos parámetros que hay que determinar son la densidad másica relativa ρ_m y el parámetro efectivo ρ_r. El primero debe medirse a partir de las técnicas de imagen y el segundo puede obtenerse mediante una simulación de MC con simetría esférica.

El número de casos estudiados es todavía bajo y limitado por el tiempo que ha durado esta investigación. El algoritmo debe verificarse para más situaciones 3D asimétricas (con DVH) en un futuro cercano y para semillas reales (no puntuales).

Además, se debe realizar un estudio en profundidad de la relación entre la composición de la heterogeneidad y el parámetro efectivo ρ_r para establecer una tabla de referencia de consenso. Los resultados de la simulación deberían compararse también con medidas experimentales usando maniquíes y semillas reales.

También es necesario estudiar cómo obtener los parámetros típicos de la calcificación (composición, densidad másica, densidad electrónica, Z efectivo, etc.) a partir de las técnicas de imagen empleadas usualmente en la rutina clínica, o cómo modificar éstas para medir dichos valores.

En conclusión, la incorporación de este modelo en la dosimetría de pacientes con heterogeneidades es factible a medio plazo, y ésta mejoraría significativamente la planificación de la dosimetría, reduciría efectos secundarios y aumentaría la calidad del tratamiento de BT.

Acknowledgments

Fernando Hueso was supported by a "Beca de Colaboración del Ministerio de Educación de España" in the Atomic, Molecular, and Nuclear Physics Department of the UVEG between 30-11-2010 and 30-06-2011.

I would like to thank my tutor Javier Vijande and the collaborators Facundo Ballester Pallarés and José Pérez Calatayud for giving me the opportunity of doing this research together with them, and also my family for their unconditional support.

References

[1] Dimos Baltas, Loukas Sakelliou - *The Physics of Modern Brachytherapy for Oncology*, 2006

[2] Omar Chibani and Jeffrey F. Williamson - *MCPI: A sub-minute Monte Carlo dose calculation engine for prostate implants*, Med. Phys. **32**, 12: 3688-3698 (Dec 2005)

[3] Guillaume Landry, Brigitte Reniers, Jean-Philippe Pignol, Luc Beaulieu, Frank Verhaegen - *The difference of scoring dose to water or tissues in Monte Carlo dose calculations for low energy brachytherapy photon sources*, Med. Phys. **38**, 3: 1526 (March 2011)

[4] Emily Poon, Frank Verhaegen - *A CT-based analytical dose calculation method for HDR ^{192}Ir brachytherapy*, Med. Phys., Vol. **36**, No. 9, September 2009

[5] G Anagnostopoulos, D Baltas, P Karaiskos, E Pantelis, P Papagiannis and L Sakelliou - *An analytical dosimetry model as a step towards accounting for inhomogeneities and bounded geometries in ^{192}Ir brachytherapy treatment planning*, 2003 Phys. Med. Biol. **48** 1625

[6] Julien Smeets - *Effects of inhomogeneities in brachytherapy - Experimental study and Monte Carlo simulation*, Department of Nuclear Metrology, Faculty of Applied Sciences - Université Libre de Bruxelles, 2008

[7] NIST - *Tables of X-Ray Mass Attenuation Coefficients and Mass Energy-Absorption Coefficients* from 1 keV to 20 MeV for Elements Z = 1 to 92 and 48 Additional Substances of Dosimetric Interest

[8] Teresa Eudaldo Puell - *Procedimientos y planificación en braquiterapia de próstata*, SEFM - Baeza 2010